

Louisiana Tech University

Louisiana Tech Digital Commons

Master's Theses

Graduate School

Winter 2-2022

Transient Thermal Response of Tissues Surrounding an Implanted Medical Device During Inductive Charging

Peter C. LeBoeuf

Follow this and additional works at: <https://digitalcommons.latech.edu/theses>

**TRANSIENT THERMAL RESPONSE OF TISSUES SURROUNDING AN
IMPLANTED MEDICAL DEVICE DURING
INDUCTIVE CHARGING**

by

Peter C. LeBoeuf, B.S, B.A

A Thesis Presented in Partial Fulfillment
of the Requirements of the Degree
Master of Science

COLLEGE OF ENGINEERING AND SCIENCE
LOUISIANA TECH UNIVERSITY

February 2022

LOUISIANA TECH UNIVERSITY

GRADUATE SCHOOL

January 7, 2022

Date of thesis defense

We hereby recommend that the thesis prepared by

Peter C. LeBoeuf, B.S, B.A

entitled **Transient Thermal Response of Tissues Surrounding an**

Implanted Medical Device During Inductive Charging

be accepted in partial fulfillment of the requirements for the degree of

Master of Science in Engineering, Mechanical Engineering Concentration



Arden Moore

Supervisor of Thesis Research



Prabhu Arumugam

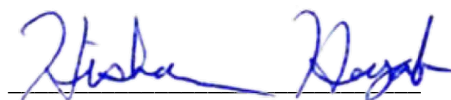
Head of Mechanical Engineering

Thesis Committee Members:

Leland Weiss

Hamzeh Bardaweel

Approved:



Hisham Hegab

Dean of Engineering & Science

Approved:



Ramu Ramachandran

Dean of the Graduate School

ABSTRACT

Inductive charging as a means of power delivery to implanted device is becoming more commonplace as increasingly sophisticated implants with higher power requirements enter clinical use. When such devices undergo inductive charging, losses within the system result in dissipated heat that must be absorbed by the surrounding tissue. The skin-mounted primary antenna and components within the implanted device such as the metal casing, battery, and secondary antenna are all susceptible to temperature increase during a charging cycle. Heating of this kind must be considered when designing modern implants utilizing this mode of power transfer in order to safeguard surrounding tissues from thermal damage, ensure patient comfort, and guarantee device longevity. The transient thermal response of tissues in the vicinity of a primary antenna and inductively charged neuromodulation implant during a charging cycle are presented in this work via a computational model incorporating device heating, tissue cooling due to blood perfusion, and multiple tissue layers. Previous studies utilizing similar numerical techniques have been conducted to investigate tissue heating, however this work seeks to transcend previous results to provide a generalized performance model across a wide range of heating conditions for a generic implanted device geometry. This will provide a useful benchmark for device manufacturers in the design of a wide variety of rechargeable implantable devices. Additionally, to maximize power transfer capability and charging performance, several thermal regulation techniques to mitigate device heating are investigated that incorporate both active and

passive cooling schemes. For cases approaching 1 W heat generation within the implanted device and antenna with no applied thermal management, local tissue temperatures did not pose a significant risk of thermal tissue damage after a two-hour charging duration. At high levels of heat dissipation, however, thermal discomfort at the skin's surface is likely to precede any actual tissue damage, thus being the limiting factor in terms of allowable heat dissipation. Comparisons against tissue temperature results for devices in clinical use proved reliability in the proposed generic model to predict maximum tissue temperatures for similar devices up to 1 W heat generation in the primary antenna and implanted device. For the four thermal regulation techniques investigated, passive standoffs at the antenna base proved most effective, decreasing max tissue temperatures by just over 1 °C.

APPROVAL FOR SCHOLARLY DISSEMINATION

The author grants to the Prescott Memorial Library of Louisiana Tech University the right to reproduce, by appropriate methods, upon request, any or all portions of this Thesis. It is understood that “proper request” consists of the agreement, on the part of the requesting party, that said reproduction is for his personal use and that subsequent reproduction will not occur without written approval of the author of this Thesis. Further, any portions of the Thesis used in books, papers, and other works must be appropriately referenced to this Thesis.

Finally, the author of this Thesis reserves the right to publish freely, in the literature, at any time, any or all portions of this Thesis.

Author Peter LeBoeuf

Date _____

DEDICATION

To the incredible faculty in the College of Engineering and Science at Louisiana Tech University – this journey would not have been possible without your constant encouragement and support.

TABLE OF CONTENTS

| | |
|--|-----|
| ABSTRACT..... | iii |
| APPROVAL FOR SCHOLARLY DISSEMINATION | v |
| DEDICATION | vi |
| LIST OF FIGURES | ix |
| LIST OF TABLES | xi |
| ACKNOWLEDGMENTS | xii |
| CHAPTER 1 INTRODUCTION | 1 |
| 1.1 Implanted Devices Overview..... | 1 |
| 1.1.1 Power Delivery to Implanted Devices | 1 |
| 1.1.2 Thermal Considerations for Implanted Devices | 2 |
| 1.1.3 Computational Model | 3 |
| CHAPTER 2 METHODS | 6 |
| 2.1 Numerical Model | 6 |
| 2.1.1 Pennes Bioheat Model | 6 |
| 2.1.2 IPG and Antenna Model | 7 |
| 2.1.3 Tissue Model..... | 10 |
| 2.1.4 Mesh Study | 13 |
| 2.1.5 Simulation Parameters and Boundary Conditions | 16 |
| CHAPTER 3 RESULTS | 19 |
| 3.1 Baseline..... | 19 |
| 3.1.1 Transient Analysis | 19 |

| | | |
|--|---|----|
| 3.1.2 | Comparisons Against Existing Devices..... | 22 |
| 3.1.3 | Max Temp. Versus Heat Dissipated | 23 |
| 3.1.4 | Tissue Damage Due to Thermal Injury..... | 25 |
| 3.2 | Thermal Management..... | 28 |
| 3.2.1 | IPG Modifications..... | 29 |
| 3.2.2 | Antenna Modifications..... | 31 |
| CHAPTER 4 CONCLUSIONS AND FUTURE WORK..... | | 35 |
| 4.1 | Conclusion | 35 |
| 4.2 | Future Work..... | 37 |
| BIBLIOGRAPHY..... | | 39 |

LIST OF FIGURES

| | |
|---|----|
| Figure 1-1: Conceptual schematic of an inductive charging setup for an implanted medical device where V_s is the time-varying source signal for the primary coil circuit. Not to scale. | 2 |
| Figure 2-1: (a) A cross-sectional view of the IMD model with overall width and thickness values as shown; (b) isometric view of final IMD solid model. | 9 |
| Figure 2-2: Isometric view of the primary antenna model with values for radius and thickness as shown. | 9 |
| Figure 2-3: Cross-sectional side view of computational domain with tissue layers and implant depth as labeled. | 12 |
| Figure 2-4: Maximum tissue temperature versus the number of mesh elements for the representative case of perfect thermal contacts and 1 W uniform internal heat generation within both the IPG and the antenna. | 14 |
| Figure 2-5: Mesh quality plot of the entire solution domain for the final selected mesh..... | 15 |
| Figure 2-6: Mesh quality plot of IPG surface for the final selected mesh..... | 16 |
| Figure 3-1: Transient thermal response of tissues surrounding the implant and primary antenna over a two hour charging duration. Solid lines and dashed lines represent the temperature on the primary antenna’s bottom surface and the IPG’s top surface, respectively. | 20 |
| Figure 3-2: Temperature distributions after one hour of charging time with (a) 0.1 W, (b) 0.5 W, and (c) 1 W heat dissipation in both the implant and primary antenna. Color scaling is in °C and is the same for all three images..... | 21 |
| Figure 3-3: Maximum tissue temperature versus dissipated power after one hour of charging time. Curves denote separate values for heat dissipation within the IPG as marked. The red horizontal line denotes the temperature threshold beyond which patient discomfort is likely. | 24 |
| Figure 3-4: IPG with exterior dimples added to increase overall surface area. | 29 |

Figure 3-5: Modified version of **Figure 3-3** showing reduction in maximum tissue to below patient comfort level as denoted by red line through reduction in IPG eddy currents.31

Figure 3-6: Temperature distribution with 1 W heat dissipation in the IPG and antenna and 0.8 W cooling ring represented with an imposed heat flux boundary condition directed as shown.32

Figure 3-7: Temperature distribution with 1 W heat dissipation in the IPG and antenna with 1 mm standoffs at the base of the antenna.33

LIST OF TABLES

| | |
|---|----|
| Table 2-1: Thermophysical Properties of IPG and Antenna Materials (All properties listed are standard atmospheric pressure and 20°C) | 10 |
| Table 2-2: Thermophysical Properties of Tissue Layers..... | 13 |
| Table 3-1: Comparison of Simulated Maximum Tissue Temperature Between Literature Values for Existing Devices and the Generalized Model from This Work..... | 23 |
| Table 3-2: Thermophysical Properties of Tissue Layers for Tissue Damage Study..... | 26 |
| Table 3-3: Maximum Temperature at Select Surfaces with Standoff Heights Ranging from 1mm to 5mm..... | 35 |

ACKNOWLEDGMENTS

This work was supported through a grant from the Louisiana Board of Regents. Special thanks to the team at Wavegate Technologies, especially Dr. Erich Wolf, Dr. Patrick O’Neal, and Charlotte Henry for their invaluable contributions. I would also like to extend my sincerest gratitude to Dr. Arden Moore for his constant guidance and support throughout this project.

CHAPTER 1

INTRODUCTION

1.1 Implanted Devices Overview

1.1.1 Power Delivery to Implanted Devices

Implanted devices are now commonplace in clinical practice and are used to treat a number of pathologies ranging from heart arrhythmia to chronic back pain. One major challenge when designing devices for continuous operation within the human body is power delivery, which traditionally was achieved percutaneously via wires perforating the skin. Further development led to the widespread use of internal batteries to mitigate the obvious risk of infection, which can supply a device such as a pacemaker with sufficient power for continued operation for ten years or more before a replacement procedure is necessary [1-3]. However, other implanted devices such as implantable cardioverter-defibrillators have higher power requirements and frequent battery replacement via invasive surgeries is required [4].

Further development in the area of power delivery to implanted devices has led to the use of inductive coupling to eliminate the need for external wires or surgical battery replacement [5-8]. Induction relies on the mutual coupling of a primary and a secondary coil, one located outside the body within a skin-mounted charging apparatus and the other within the implanted device itself. A high frequency alternating current is passed through the primary coil (also sometimes referred to as the antenna coil) which generates a

fluctuating magnetic field in its vicinity. This time-varying magnetic flux induces a current flow within the secondary (receiving) coil that can be used to recharge the IMD's internal battery via a rectifying circuit [6]. The frequency at which the primary coil is charged varies, traditionally lying in the low MHz range for devices with cm-sized links. Smaller devices, however, may have link frequencies in the 100 MHz range and higher [5]. A simplified schematic of a typical wireless induction charging arrangement for an implanted device is shown in **Figure 1-1**.

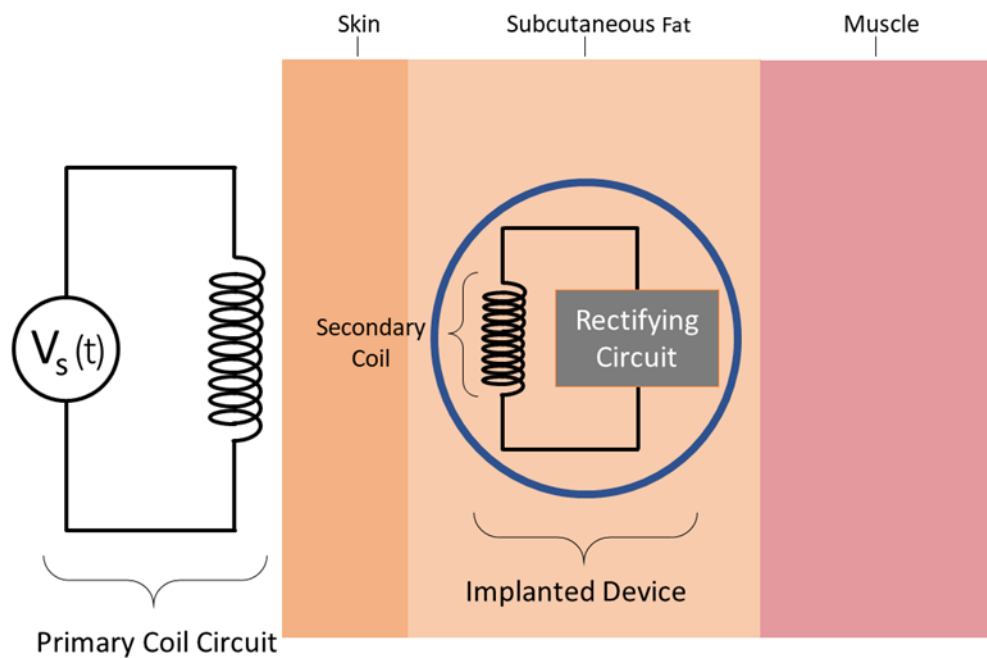


Figure 1-1: Conceptual schematic of inductive charging setup for an implanted medical device where V_s is the time-varying source signal for the primary coil circuit. Not to scale.

1.1.2 Thermal Considerations for Implanted Devices

Inductive charging as a means of power transfer to implanted devices comes with some risk of thermally-induced tissue damage due to heat dissipation from both the skin-mounted primary antenna and the IMD. Several factors can influence the rate of heat

dissipation to surrounding tissues during a charging cycle, including the particular geometry of the induction coils, coil material, and rate of power transfer [9]. In addition to temperature increase within the primary and secondary coils due to their finite resistivity, other sources of heat within the IMD can include heating of the internal circuitry required to rectify the incoming AC signal, and induced currents in metal components such as the outer metallic housing. The antenna module alone can experience heating comparable to the entire IMD itself due to the larger primary coil contained within a casing that rests on the surface of the skin during charging. For both coils, the amount of heat dissipated depends on the rate of power transfer during a charging cycle. A faster charging rate is advantageous to reduce charging time and ensure patient satisfaction and compliance yet leads to increased heating and possible discomfort or tissue damage. Utilizing the highest charging rate while limiting device heating to avoid thermal tissue damage is therefore a pressing need in the field of inductively charged implantable devices. Because the onset of thermal discomfort may occur well before any actual tissue damage, patient comfort is equally important to consider to ensure proper charging schedule compliance.

1.1.3 Computational Model

Previous studies investigating the thermal effects of neuromodulation devices undergoing inductive charging have been conducted with particular success. Earlier work has investigated the design and optimization of improved charging systems for implanted devices that greatly increase link efficiency, incorporating advancements such as 3-D printed spiral induction coils and active primary coil frequency control for thermal management [5,6]. Animal experiments were performed to verify numerical predictions of temperature rise near implanted devices undergoing inductive charging and have shown

excellent agreement [10]. Similar models to verify *in-vivo* experimental results have also been extended to the human case to ascertain possible thermal tissue damage within neuromodulation implants [11]. Numerical solutions to Eq. (1) have also been used to assess certain therapies such as radiofrequency tumor ablation and similar hyperthermia treatments [12,13].

There currently exists several commercial neuromodulation devices with inductive charging capabilities that have entered clinical use, each with their own unique size, shape, materials, and charging protocols that render summary statements regarding the thermal effects on tissues for such devices difficult given each of their different heat dissipation characteristics. This work seeks to provide a broader understanding in the potential for inductively charged IMDs to cause tissue damage across a wide range of heating conditions by investigating an IMD of generic geometry, providing much wider applicability and utility to the design of a variety of rechargeable implantable devices. With information regarding the thermal effects of a charging cycle on the tissue temperature surrounding an implanted device, IMD researchers and designers may be able to evaluate the possibility of thermal tissue damage and assess a particular system architecture to compensate early in the design cycle, saving valuable time and effort. In this study, a computational model based on numerical solutions to the Pennes bioheat equation is used to evaluate the thermal response of tissues surrounding a representative IMD during an inductive charging cycle under various charging conditions and heat dissipation rates. Further, several thermal regulation strategies are proposed to improve system performance and allow for higher rates of power transfer. A transient thermal model is proposed to simulate the charging cycle for an internal pulse generator (IPG) typical of current neuromodulation systems.

Using the bioheat transfer module within COMSOL Multiphysics, timewise variations of local tissue temperature for charging times of up to two hours and volumetric heat dissipation rates ranging from 0.1 to 1W within the charging antenna and implant are studied under various combinations of heating conditions. Finally, the potential for thermal tissue damage is investigated for all transient and steady-state tissue temperature results.

CHAPTER 2

METHODS

2.1 Numerical Model

2.1.1 Pennes Bioheat Model

The need for insights into the relationship between heat dissipation during charging and the resulting temperature rise in surrounding tissues lends itself to the use of computational modeling to simulate the body's thermal response for IMD heat dissipation under varying conditions. This is especially true during the design of a new IMD, where such relationships may not be predictable early in the design cycle. The mechanisms of heat transfer within the human body and thermal transport through living tissues remains a topic of continued research and has been investigated for over a century with Bernard being the first to conduct an experimental study in 1876 [14,15]. Understanding the role of blood in heat transfer within living tissues presents a particular challenge due to heterogeneous vasculature, particularly within the capillary bed. Such complex geometries render a purely analytical solution for modeling temperature rise within tissues impossible, however numerical simulations can provide insight into how heat dissipation affects surrounding tissues with known thermal properties by modeling discretized regions of tissue and solving the bioheat equation according to the Pennes approximation:

$$\rho C_p \frac{\partial T}{\partial t} - \nabla \cdot (k \nabla T) = \rho_b w_b C_{p,b} (T_a - T) + q_m \quad \text{Eq. 2-1}$$

Here, ρ is the tissue density, C_p is the tissue specific heat, k is the tissue thermal conductivity, w_b is the blood perfusion rate, $C_{p,b}$ is the blood specific heat, ρ_b is the blood density, q_m is the metabolic heat generation per unit volume, T_a is the arterial blood temperature, $\partial T/\partial t$ is the rate of temperature change, and T is the dependent variable. American physician and clinical researcher Harry Pennes introduced this mathematical model in 1946 to describe the role of local blood flow as it relates to tissue temperature and metabolic heat production. Using the classic Fourier law of heat conduction, his model remains the gold standard in terms of modeling heat conduction in tissues and has provided the theoretical framework for hundreds of papers over the last 50 years [16]. Due to its linearity, the Pennes bioheat model lends itself well to numerical simulation and can accurately simulate heat transfer within tissues with close agreement to experimental results [17].

2.1.2 IPG and Antenna Model

The IMD model created for this study most closely resembles a typical internal pulse generator (IPG) used in neuromodulation systems, however applicability of these results is not limited to that device type. To create a representative IMD model within COMSOL that was simultaneously device-neutral and realistic within the class of typical neurostimulation devices, an iterative approach was followed within COMSOL's built-in modeling tool to create a three-dimensional solid beginning with a simplified, solid ellipsoid shape useful for verifying boundary conditions during preliminary test simulations. The final modeling iteration, using dimensions taken via an averaging of values across commercial offerings, included a 0.675mm outer titanium shell, battery compartment, and two adjacent compartments housing device circuitry, shown in **Figure**

2-1. The internal cavities of the IMD were modeled as air due to its low thermal conductivity and ability to fill void space between components. Prior validated usage of such a technique as a conservative thermal estimate was found within literature for similar bioheat simulations [18].

The antenna structure modeled considers only a volumetric heat source within disk-shaped elastomer casing in perfect alignment with the IPG. This method was chosen to create an antenna model that was equally neutral and realistic across various antenna types on the market, neglecting complex internal components with insignificant effect on overall thermal response to heating. Prior study has included the internal structure to varying degrees in their numerical models. Lovik, et al. [19] and Abraham, et al. [20] considered a proprietary antenna for the Medtronic Restore™ device consisting of ten different materials in fifteen separate parts and accounted for internal heat transfer due to conduction and natural convection in air gaps. Plourde, et al. [11] and Stark, et al. [21], however, considered only the antenna's internal copper transmitting coil within an elastomer casing. The charging antenna model is shown in **Figure 2-2**. The thermophysical properties of the IMD and antenna materials are governed by piecewise functions within COMSOL as a function of temperature. These values are listed in **Table 2-1** [11].

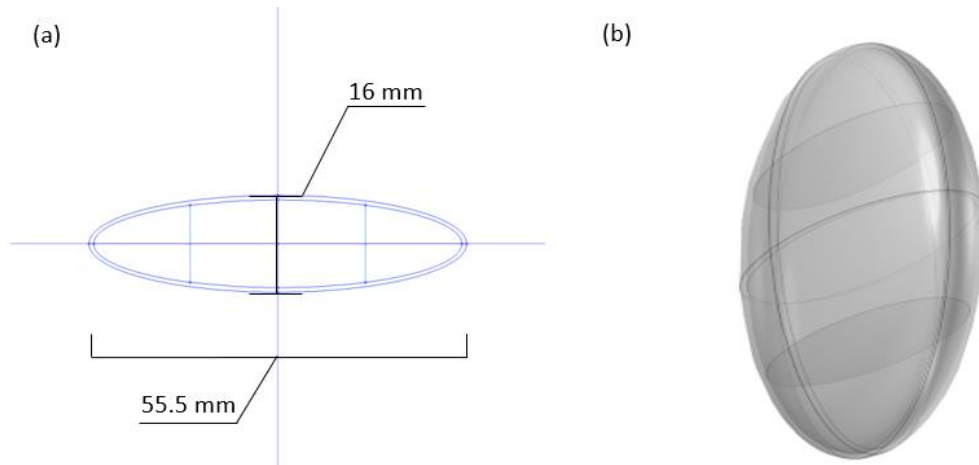


Figure 2-1: (a) A cross-sectional view of the IMD model with overall width and thickness values as shown; (b) isometric view of final IMD solid model.

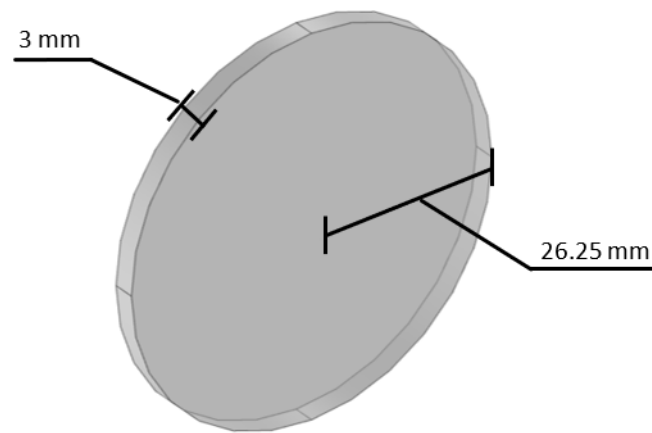


Figure 2-2: Isometric view of the primary antenna model with values for radius and thickness as shown.

Table 2-1: Thermophysical Properties of IPG and Antenna Materials
(All properties listed at standard atmospheric pressure and 20° C)

| Component | Thickness (mm) | Density (kg/m ³) | Thermal Conductivity (W/m·K) | Specific Heat (J/kg·K) |
|------------------|----------------|------------------------------|------------------------------|------------------------|
| <u>IPG</u> | | | | |
| Titanium Shell | 0.675 | 4690.5 | 21.3 | 509.9 |
| Air (internals) | N/A | 1.2 | 0.024 | 1005 |
| <u>Antenna</u> | | | | |
| Elastomer Casing | 3 | 1250 | 3.0 | 1750 |

2.1.3 Tissue Model

The lateral distance between the adjacent primary coil located within the skin-mounted antenna and secondary coil housed in the IMD greatly effects charging efficiency and thus implant depth for current neuromodulation systems is typically limited to 1-3 cm [22]. This distance represents a balance between charging efficiency and minimization of tissue temperature rise, particularly in the tissue gap between these two components during a charging cycle. Previous work studied the effect of implant depth and tissue temperature rise during charging for various implant depths and showed nontrivial thermal challenges in terms of tissue damage for a 1.5 cm implant depth for at least one specific similar device [11]. For our purposes, this implant depth will be used to assess possible tissue damage for various heat dissipation rates. Coil misalignment is another important factor in charging efficiency for induction systems. Lovik, et al. [23] investigated the effect of antenna and secondary coil misalignment and tissue temperature rise and found an important correlation

between antenna alignment and maximum tissue temperature; however, the simulated neuromodulation device belonged to an earlier generation more susceptible to coupling efficiency decrease during misalignment that would increase power to compensate [11,23]. Safeguards exist in current generation devices that limit charging rate even in the case of coil misalignment. Plourde, et al. [11] investigated the effect of a 2 cm lateral misalignment with a constant heating rate and found little correlation between antenna misalignment and the resulting tissue temperature distribution in the numerical model. Given these findings, only a perfectly aligned antenna was considered for the following numerical studies.

It is important to note that there is a difference between the total power associated with the charging process and the value of heat dissipation. The relationship between charging rate and heat dissipation is specific to the charging circuit within the device, even for the same battery capacity. A well-designed, high-end charging circuit would have less heating than another circuit even for the same charging rate and battery size. Since the goal of this work is to generalize the thermal response to the degree of heat dissipation, such device-specific limitations were deemed outside the scope of this work. If a practicing engineer wished to apply our results to their own device design, they only need to know the relationship between charging rate and heat dissipation within their circuit to be able to link charge rate, charge time (according to battery capacity), and expected tissue temperature.

A cross-sectional view of the simulation domain comprised of three tissue layers is shown in **Figure 2-3**. The topmost layer represents the skin, followed by subcutaneous fat tissue and finally muscle. There is some ambiguity regarding the best values to use for the thickness of tissue layers below the skin surface, as these vary slightly from patient to

patient. For our purposes, the thermophysical properties and tissue layer thicknesses were chosen to maintain consistency with similar preceding numerical studies [11,19,20,21] to best facilitate the comparison of results between the preceding device-specific works and the generalized approach in this work. Temperature gradients parallel to the skin surface are expected to be small compared with temperature gradients along the surface normal vector on account of device geometry, therefore the model's dimensional boundary conditions are set to be five times the IPG's major radius. Subsequent results will later support this assumption. The thermophysical properties of the simulated tissues are listed in **Table 2-2**. These values are built into COMSOL and agree with relevant scientific literature [11,19,20,21,24].

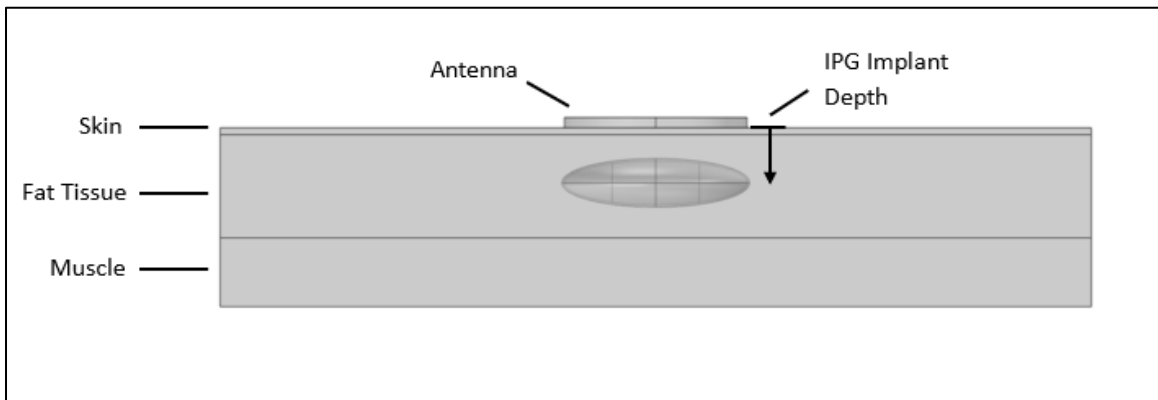


Figure 2-3: Cross-sectional side view of computational domain with tissue layers and implant depth as labeled.

Table 2-2: Thermophysical Properties of Tissue Layers

| Tissue Type | Thickness (mm) | Density (kg/m ³) | Thermal Conductivity (W/m·K) | Specific Heat (J/kg·K) |
|-------------|----------------|------------------------------|------------------------------|------------------------|
| Skin | 2 | 1109 | 0.37 | 3391 |
| Fat | 30 | 911 | 0.21 | 2348 |
| Muscle | 20 | 1090 | 0.49 | 3421 |

2.1.4 Mesh Study

A mesh convergence study was performed prior to running any simulations for the IPG model under various charging conditions to ensure adequate, mesh-independent simulation results. A tetrahedral, Delaunay-based mesh was created using COMSOL's integrated mesh generator for a representative test case assuming perfect thermal contact between the IPG and surrounding tissue and between the primary antenna's surface and the skin layer, with 1 W uniform heat generation within both the IPG battery compartment and the primary antenna. The mesh density was progressively refined until further refinement yielded negligible difference in the temperature solution at select points within the solution domain where temperature gradients were high, namely the region between the primary antenna and IPG. **Figure 2-4** displays results for this test case, using values for maximum tissue temperature. Solution convergence occurred at just over 225,000 mesh elements at which point values for maximum tissue temperature showed mesh-independent results at just under 43.49°C. The mesh created for the final model exceed this threshold consisting of 263,365 mesh elements.

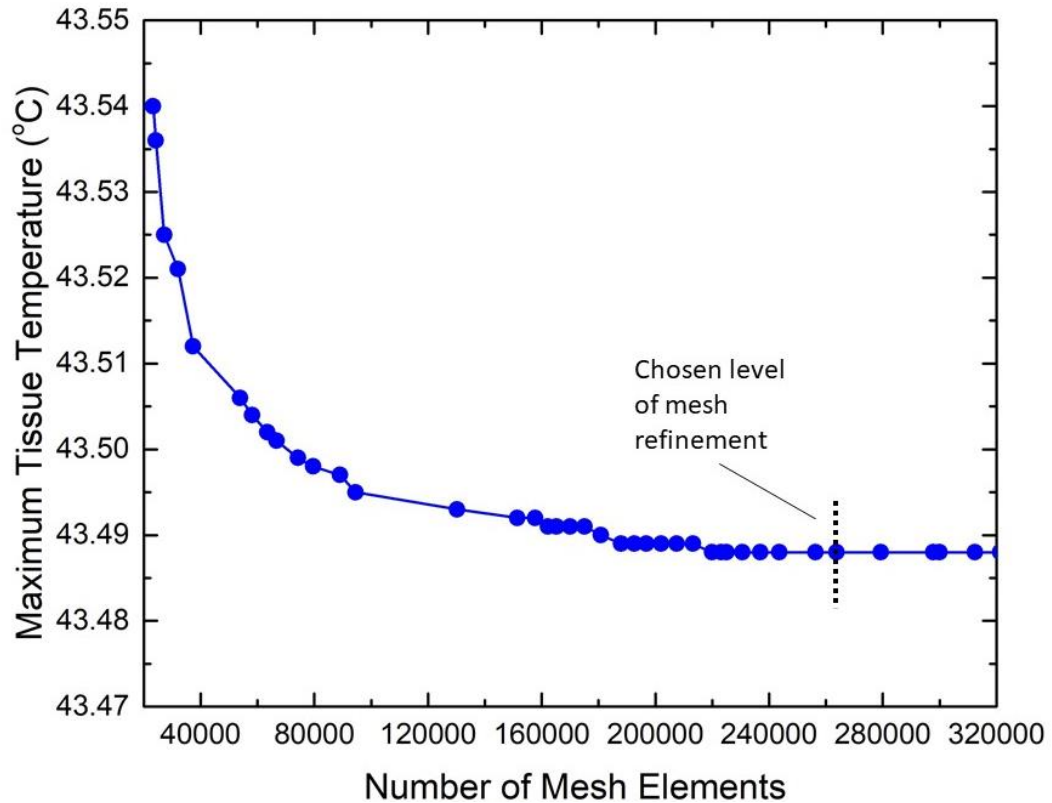


Figure 2-4: Maximum tissue temperature versus the number of mesh elements for the representative case of perfect thermal contacts and 1 W uniform internal heat generation within both the IPG and the antenna.

A mesh quality study was also performed to ensure maximum regularity in mesh elements' shapes and to avoid inverted or otherwise distorted elements that could cause convergence issues and inaccurate results. COMSOL allows for visualization of mesh elements to assess element quality based on element skew, one of several quality measures that compares the angles over all edges of 3D mesh elements within the solution domain and compares these values to the ideal corresponding element, assigning a value between zero (worst quality) and one (best quality). **Figure 2-5** and **Figure 2-6** display mesh elements within the solution domain highlighted according to their quality. COMSOL recommends a minimum element quality above 0.1 to ensure accurate simulation results for default solver settings

[25]. The minimum mesh quality was 0.143 with an average mesh quality of 0.630 for the final mesh used in this study.

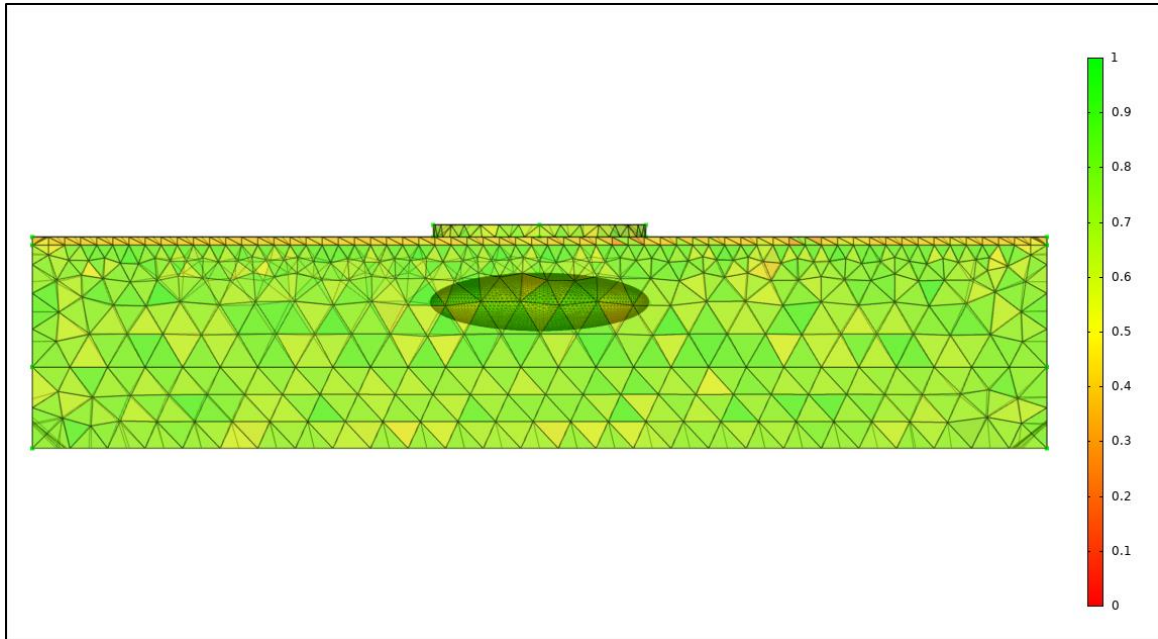


Figure 2-5: Mesh quality plot of the entire solution domain for the final selected mesh.

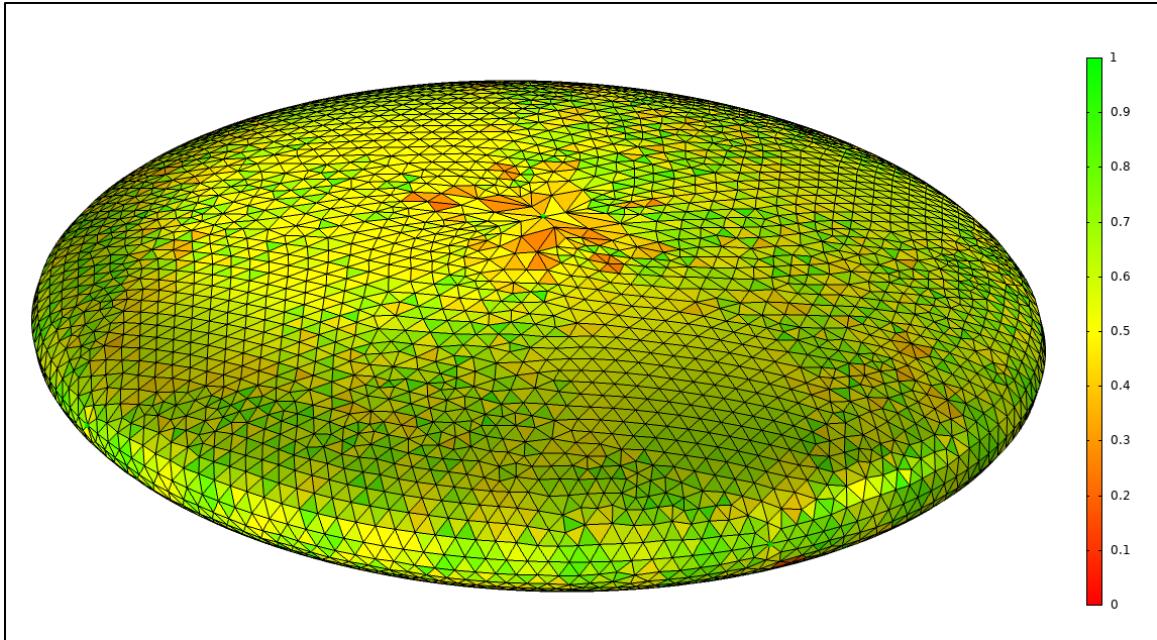


Figure 2-6: Mesh quality plot of IPG surface for the final selected mesh.

2.1.5 Simulation Parameters and Boundary Conditions

The foundation for the computational approach used here is a numerical solution on a node-by-node basis to the bioheat equation according to the Pennes approximation as given in **Eq. 2-1**. The first term on the right-hand side of the equation describes the convective cooling effect of blood perfusion, controlled by several variables including arterial blood temperature, blood specific heat, blood perfusion rate, and blood density. The blood perfusion rate, w_b , is characterized as the volumetric flow rate of blood per volume of tissue and depends on several variables including tissue type. Adipose blood tissue flow is particularly variable, increasing up to 20-fold during exercise or after a meal is eaten. For our purposes, an average value of 10 mL of blood per 100 g of fat tissue per minute was chosen based on guidance from literature [26]. This value is slightly above normothermic blood perfusion rates due to the vasodilative effect of temperature increase in tissues [27]. Arterial blood temperature T_a was set at a normal body temperature of

310.15 K. Blood specific heat $C_{p,b}$ and density ρ_b were defined as 3840 J/(kg·K) and 1060 kg/m³, respectively [28,29]. Metabolic heating was specified to be 250 W/m³, 1300 W/m³, and 500 W/m³ within subcutaneous fat tissue, skin, and muscle layers respectively [19]. At the upper surface of the solution domain including the outer skin layer and antenna, a combined radiation and convective heat transfer coefficient was defined of 10 W/(m²·K) per guidance from literature [11,19,20]. This corresponds to a typical ambient condition at room temperature indoors at 20°C, neglecting any small timewise variations. Attention was focused on determining the effect of varying levels of thermal contact resistance between the IPG and surrounding tissue on maximum tissue temperature. Preliminary simulations were conducted with values for thermal contact resistance at all device-tissue interfaces ranging from 0.0001 to 0.001 m²·K/W including a case of perfect thermal contact i.e., zero thermal contact resistance [30]. Negligible difference was observed in the maximum tissue temperature for heating within the IPG with variation in thermal contact resistance. This agrees with prior work on this subject [11,31] and thus thermal contact resistance was not included in subsequent simulations.

A constant core body temperature was imposed at the bottom surface of the tissue model. All outer surfaces of the solution domain were defined as being adiabatic considering that horizontal temperature gradients are expected to be small, as discussed above. This assumption is supported by tissue temperature results to follow. Initial values for temperature were determined by imposing the aforementioned boundary conditions without any heat generation within the primary antenna or IPG then inputting the results of a steady-state solution to the tissue temperature distribution on a node-by-node basis as the starting point for the transient solutions that include device heating to follow. Separate

volumetric heat sources were defined within the center compartment of the IPG model which houses the battery and charging circuitry and within the primary antenna housing to account for heat dissipation during inductive charging. Using this simulation scheme, the effect of varying combinations of heat dissipation from the IPG and antenna on the tissue temperature distribution can be investigated. No blood perfusion within solid components was allowed and continuity of temperature and heat flux was imposed at all boundaries.

CHAPTER 3

RESULTS

3.1 Baseline

3.1.1 Transient Analysis

A series of transient analyses were performed to study the tissue temperature response for heat dissipation rates of 0.1, 0.5, and 1 W occurring simultaneously in both the implant and antenna. These values were chosen based on information gathered on existing commercial inductively-charged neuromodulation systems that show heat dissipation rates in practice typically between 0.2 W and 1 W for both the primary antenna and implanted IPG during normal charging. Heat dissipation rates in the primary antenna are expected to be comparable or higher than that of the IPG in most cases [11,19,20,32]. The assignment of equal values of heat dissipation in both solid components and the range of 0.1 W to 1 W therefore represents a set of test cases that are meaningful in terms of hardware currently in clinical use, and valuable for initial analysis of transient tissue temperature response during charging of a generalized IMD. Results for the transient thermal response of the tissue over a two-hour charging duration at these charging conditions are plotted in **Figure 3-1**. For simplicity, only the maximum calculated tissue temperatures for the selected surfaces are plotted in **Figure 3-1** over the two-hour charging duration, while **Figure 3-2** displays the steady-state temperature distributions associated

with each of the charging conditions and the corresponding hot-spot location and temperature. Steady-state conditions are reached after approximately one hour of charging at which point curves for maximum tissue temperature level off as seen in **Figure 3-1**. **Figure 3-2** shows that as the heat dissipation rate increases, the location of the maximum tissue temperature moves from the IPG surface to the antenna surface, demonstrating that the location of the hottest temperature is a function of heat dissipation rate. **Figure 3-2 (c)** in particular shows that the tissue located between the IPG and antenna is the most prone to experiencing significant temperature rise at high levels of heat dissipation.

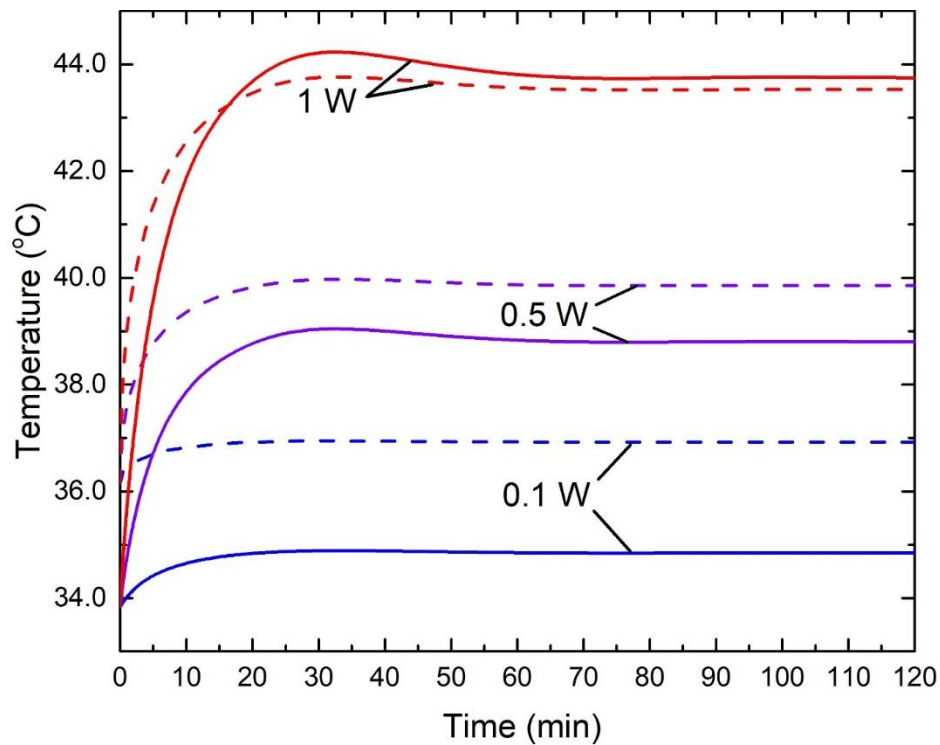


Figure 3-1: Transient thermal response of tissues surrounding the implant and primary antenna over a two hour charging duration. Solid lines and dashed lines represent the temperature on the primary antenna's bottom surface and the IPG's top surface, respectively.

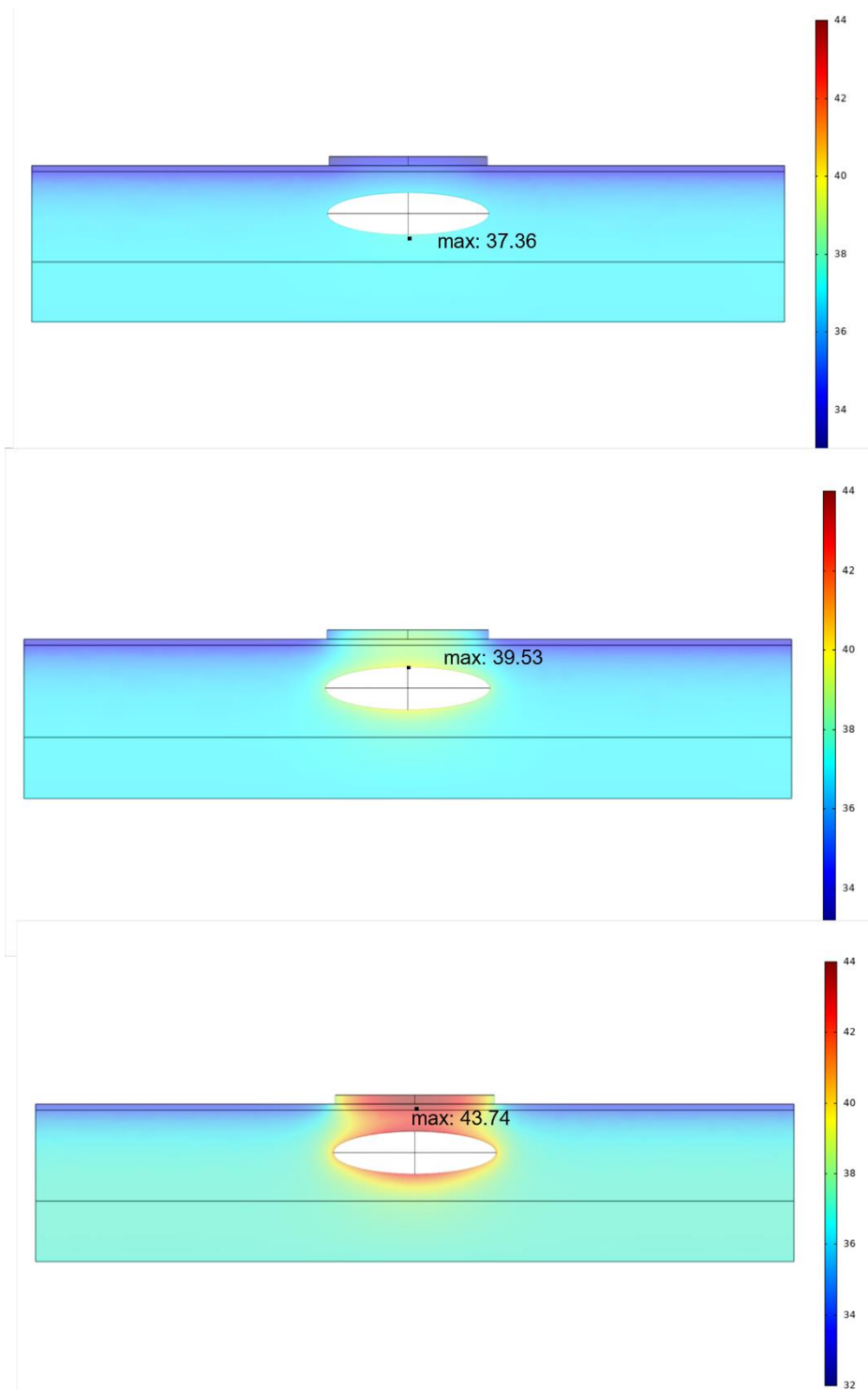


Figure 3-2: Temperature distributions after one hour of charging time with (a) 0.1 W, (b) 0.5 W, and (c) 1 W heat dissipation in both the implant and primary antenna. Color scaling is in °C and is the same for all three images.

3.1.2 Comparisons Against Existing Devices

Comparisons against results from several device-specific references in literature were made to assess the robustness of the employed generalized numerical model against values for measured heating rates and simulated maximum temperatures for existing devices on the market to verify the accuracy and utility of these results. Specifically, the comparison was made between values of maximum tissue temperature found in literature for existing devices with known heat dissipation rates and the results of our generalized model with these same heat dissipation rates applied. Values for heating rate and maximum tissue temperature for existing devices were found for the Medtronic Restore [19], Medtronic Intellis [11], Medtronic Restore Ultra [20], and the ANS Eon [32]. These values have been summarized in **Table 3-1** together with the results from the generalized model in this work. As can be seen, the results of the model are within 1 °C of those reported, which supports the use of the generalized model and the applicability of its results to IMDs of various type and charging conditions.

Table 3-1: Comparison of Simulated Maximum Tissue Temperature Between Literature Values for Existing Devices and the Generalized Model from This Work

| Device | Heat Dissipation: IPG (W) | Heat Dissipation: Antenna (W) | Reported Max Tissue Temp. (°C) | This Work's Max Tissue Temp. (°C) |
|-------------------------|---------------------------|-------------------------------|--------------------------------|-----------------------------------|
| Medtronic Restore | 0.233 | 0.200 | 39.2 [19] | 38.2 |
| Medtronic Restore Ultra | 0.253 | 0.395 | 38.5 [20] | 38.4 |
| Medtronic Intellis | 0.637 | 0.573 | 39.9 [11] | 40.7 |
| ANS Eon | 0.670 | 0.343 | 41.1 [32] | 40.6 |

3.1.3 Max Temp. Versus Heat Dissipated

With the validation provided through the comparisons in **Table 3-1**, attention was turned to producing a range of results with wide-range applicability for IMDs under various charging/heating conditions to provide a valuable reference for IMD researchers and developers to determine approximate corresponding maximum tissue temperature. Simulations were performed considering various combinations of heat dissipation within the IPG and antenna for heat dissipation rates between 0.1 W and 1 W. In this way, the simplifying condition of comparable power dissipation in the two devices was removed for these simulations. **Fig. 3-3** summarizes these results and represents potentially the most impactful outcome of this work. IMD researchers and designers can leverage the results in **Figure 3-3** to predict the maximum tissue temperature during charging early in their design cycle before committing the time and effort to a more detailed, device-specific investigation, or to evaluate the likelihood of damage or patient discomfort from an existing IMD of known power dissipation characteristics.

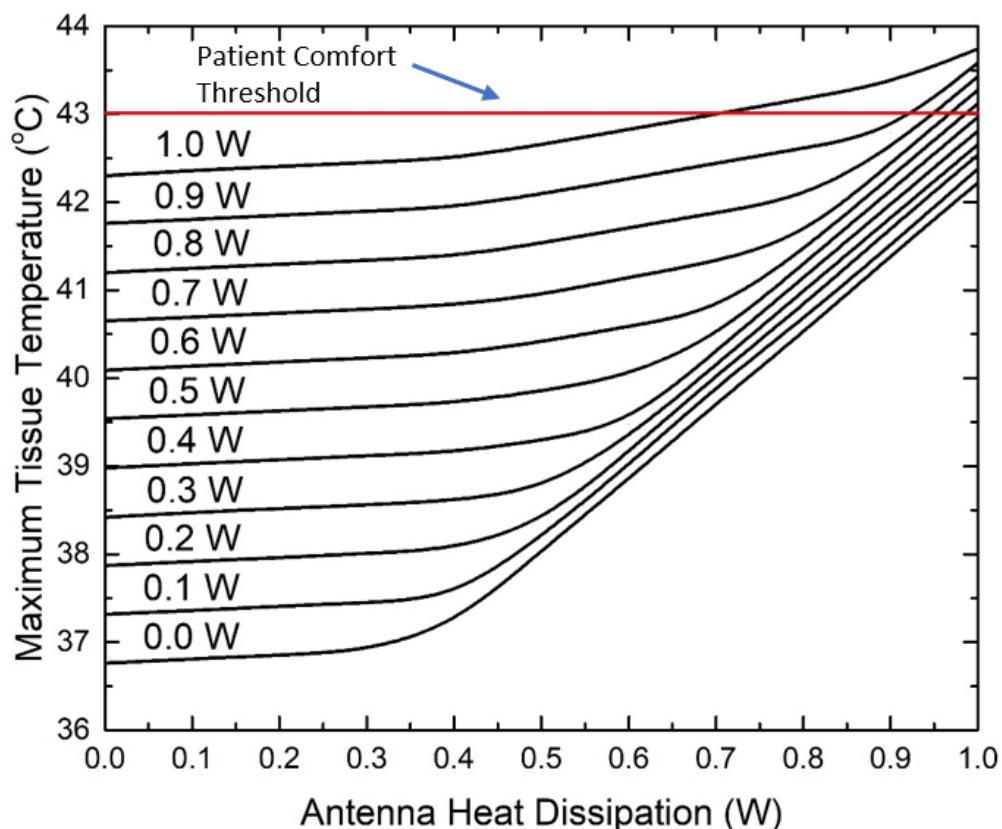


Figure 3-3: Maximum tissue temperature versus dissipated antenna heat after one hour of charging time. Curves denote separate values for heat dissipation within the IPG as marked. The red horizontal line denotes the temperature threshold beyond which patient discomfort is likely.

Several important insights can be drawn from the results as presented in **Figure 3-3**. First, it appears that for heat dissipation rates below 0.35 W in the primary antenna, tissue temperature is very weakly dependent on the rate of heat dissipation in this component. In this range, tissue temperature is seen rather to be a function mostly of IPG heat dissipation, increasing steadily with IPG heating. Outside this region, values for maximum tissue temperature are seen to dramatically increase with primary antenna heat dissipation for curves of constant IPG heat dissipation. A sharp “knee” can be seen along each curve denoting the transition into this regime, visibly more prominent for lower values of IPG heat dissipation. Various curves coalesce within this regime, and while still showing

a steady increase in tissue temperature with increased IPG heat dissipation, primary antenna heat dissipation is shown in **Figure 3-3** to be the major driving force for tissue temperature increase in this region. The ability to visualize these relationships is valuable not only from a theoretical point of view, but also from a design perspective. Identifying major contributors to maximum tissue temperature can guide what parts of the IMD system are targeted for thermal management. For example, suppose a given IMD system's heat dissipation characteristics are such that it falls on the left region of **Figure 3-3**. In this scenario, efforts to reduce heat dissipation will pay greater dividends towards minimizing tissue temperature if focused on the IPG itself, it being the major contributor to maximum tissue temperature. Conversely, an IMD system whose heat dissipation profile is found to lie in the rightmost regime would benefit most from efforts to reduce the heat dissipation in the primary antenna, rather the IPG itself.

3.1.4 Tissue Damage Due to Thermal Injury

With maximum tissue temperature data now available under various charging conditions, possible tissue damage due to thermal injury can be assessed using the Thermal Damage functionality within COMSOL. This tool calculates the degree of tissue damage using the Arrhenius integral injury method to assign a value between zero (no damage) and one (tissue necrosis has occurred) by integrating Eq. (2) over a specified time interval.

$$\Omega(t) = A \int_0^t e^{\frac{-E_A}{RT}} d\tau \quad \text{Eq. 3-1}$$

where E_A is the activation energy in J/mol, \bar{R} is the universal gas constant, and A the frequency factor (or so-called pre-exponential constant) in 1/s. These material properties specific to each tissue layer are built into COMSOL and are listed in **Table 4**.

Table 3-2: Thermophysical Properties of Tissue Layers for Tissue Damage Study

| Tissue Type | Activation Energy (J/mol) | Frequency Factor (1/s) |
|-------------|---------------------------|------------------------|
| Skin | 4.71×10^{-5} | 4.58×10^{72} |
| Fat | 1.3×10^5 | 4.43×10^{16} |
| Muscle | -- | -- |

The equivalent dosimetry method (CEM43°C) is typically employed for lower temperature applications while the Arrhenius method is preferred for higher temperature applications such as modeling tumor ablation. Our rationale for employing the integral method is twofold: First, the thermodynamic and physical processes from which both methods originate are very similar – namely, Arrhenius’ experimental observations in the 1880’s [33]. Studies have demonstrated a strong correlation between the CEM43°C values calculated at the basal skin layer and the predicted degree of tissue damage from the injury integral for a numerical model very similar to ours [34]. Additionally, others endeavoring to evaluate possible tissue damage from low-level thermal exposure from implanted devices have used the integral model with success [19,21]. In the case of [21], both methods were used and produced consistent results. Second, the numerical software used to carry out our simulations contained built-in tissue damage evaluation software based on the Arrhenius model, therefore this method was favored in order to streamline results within a single software interface. As a worst case, **Eq. 3-1** was evaluated at three locations within the solution domain over a two hour charging duration given 1 W heating within both the

IMD and the primary antenna which produced a maximum Ω of 0.11. There is a general consensus that tissue damage is likely to occur for values of Ω on the order of one. Hence, this result suggests damage to tissues surrounding the IMD's casing and the antenna is unlikely for these charging durations and charging conditions and any at lower heat dissipation levels. The results agree with findings in literature for the four previously mentioned devices that were investigated, as none of them were found to cause tissue temperature elevations significant enough to cause tissue damage during clinical use. In practice, heat dissipation rates in real devices could exceed 1 W in an attempt to increase charging rate and shorten the total charging time. However, modern devices contain safeguards to throttle power transfer in the case of device over-heating.

Patient comfort during charging is also important to consider despite the low risk of thermally induced tissue damage under normal operation for modern inductively charged neuromodulation devices. Even if the tissue temperatures experienced during charging are not high enough to cause tissue damage, a prolonged uncomfortable sensation may cause the patient to halt charging prematurely or stop using the therapeutic device due to dissatisfaction. Numerous studies have been conducted to quantitatively assess the threshold of perceived pain for warm electronic devices in contact with human skin. These studies have identified several factors that can contribute to an individual's sensation of heat including age, gender, local ambient temperature, surface material, etc. These studies also indicate that the normal threshold for the onset of a warm sensation occurs for object surfaces in contact with the skin between 33°C and 35°C [35]. There is significant variability in the results of studies seeking to determine the exact temperature at which pain is perceived, mainly due to variation in patient response, testing procedures, and the fact

that some body sites are more sensitive to heat than others. The threshold for thermal discomfort for hot surfaces in contact with the skin seems to be lowest for the face and chest, followed by the trunk, and highest in the hands, arms, and legs. *Defrin et al.* [36] determined that for chest skin, the average pain threshold was 42°C. *Zhang et al.* [37] found 43°C to be the average limit for thermal discomfort. Henriques and Moritz [33] were the first to establish a time-temperature relationship for the perception of pain and superficial dermal burns in adult human skin. These plots and burn damage integral proposed by Henricque and Moritz have served as the basis for virtually all efforts to quantify thermal damage in tissues, which identified 44°C as the limit for burn injury in the upper dermis. Stoll [38] identified 43.2°C as the threshold for pain receptors in the skin mediating pain response. These results are supported by others [39,40] studying the skin's response to thermal radiation. For our purposes, 43°C will be considered as the maximum acceptable tissue temperature at the antenna-skin interface to avoid patient discomfort. **Figure 3-3** reflects this imposed limit as a horizontal line at 43°C above which the authors recommend operation be avoided, particularly in the primary antenna. The limit for heat dissipation within the primary antenna can be seen graphically in **Figure 3-3** for IPG heat dissipation rates above 0.7 W. Specifically, at heat dissipation rates of 0.7 W, 0.8 W, 0.9 W, and 1 W in the IPG, primary antenna heat dissipation should be limited to approximately 0.975 W, 0.95 W, 0.9 W and 0.75 W, respectively, to avoid potential patient discomfort.

3.2 Thermal Management

Several novel thermal management techniques not found elsewhere in literature were investigated for their potential impact on reduction of maximum tissue temperature at high levels of component heat dissipation. Two avenues of thermal management were

considered, targeting either the IPG device or skin-mounted antenna. Both active and passive cooling schemes were explored, and their efficacy evaluated against baseline thermal results as outlined previously.

3.2.1 IPG Modifications

Alteration of the IPG geometry was considered first as a preliminary effort to maximize surface area and encourage heat transfer to surrounding tissues. This passive scheme was deemed attractive from a device manufacturer point of view as a relatively simple means of improving thermal performance early in the design cycle with minimal added complexity and without compromising device function. To increase surface area on the exterior of the IPG device, many small dimples similar to that on the outside of a golf ball were incorporated into the thermal model considering perfect contact between the tissue and IPG surface. This edited geometry is presented in **Figure 3-4**.

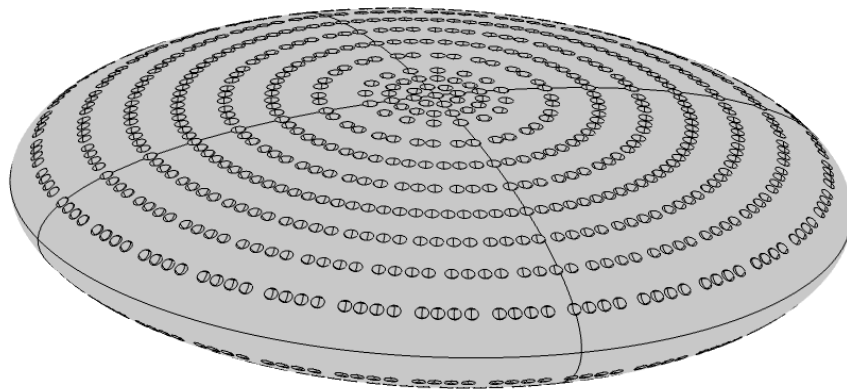


Figure 3-4: IPG with exterior dimples added to increase overall surface area.

Thermal gains resulting from modification of the exterior of the IPG device proved insignificant when compared to baseline thermal results. At 1 W heat dissipation in the IPG and antenna considering an unmodified IPG, the maximum tissue temperature was calculated at 43.7 °C. The addition exterior dimples proved relatively ineffective in

reducing maximum tissue temperature with a $0.1\text{ }^{\circ}\text{C}$ reduction for a 11 percent increase in surface area. Considering the operating conditions of the IPG device, a change of geometry was only expected to offer substantive benefits if perfusion/convective cooling was significant or if thermal interface resistance was a limiting factor, both of which were shown previously to have minimal contributions to overall thermal tissue response based on the Pennes model. Additionally, very small dimples are not likely to totally conform to surrounding tissue thus negating the desired effect with this method. Therefore, this passive cooling scheme was deemed unlikely to provide any significant thermal gains during charging, and further pursuit is unlikely.

Eddy currents generated in the outer metal casing of an implant due to the local magnetic field flux produced by the primary antenna coil can be a major contributor to overall heat dissipation for neuromodulation implants. A change of casing material from titanium to another material such as ceramic could represent significant gains in lowering maximum tissue temperature. Based on evidence found in literature for a similar device at the same implant depth, total heat dissipation from the IPG device could be reduced from approximately 1.1 W to 0.47 W if eddy currents were drastically decreased or eliminated in the casing by this change in material [11]. Considering the current simulation techniques employed in this study did not incorporate the electromagnetic interactions necessary to capture this decrease in eddy current generation, comparison of maximum tissue temperatures from 1 W heat dissipation in the IPG to roughly 0.5 W as shown in **Figure 3-5** suffice as a judge against baseline results, showing a promising reduction in tissue temperature to below the patient comfort threshold.

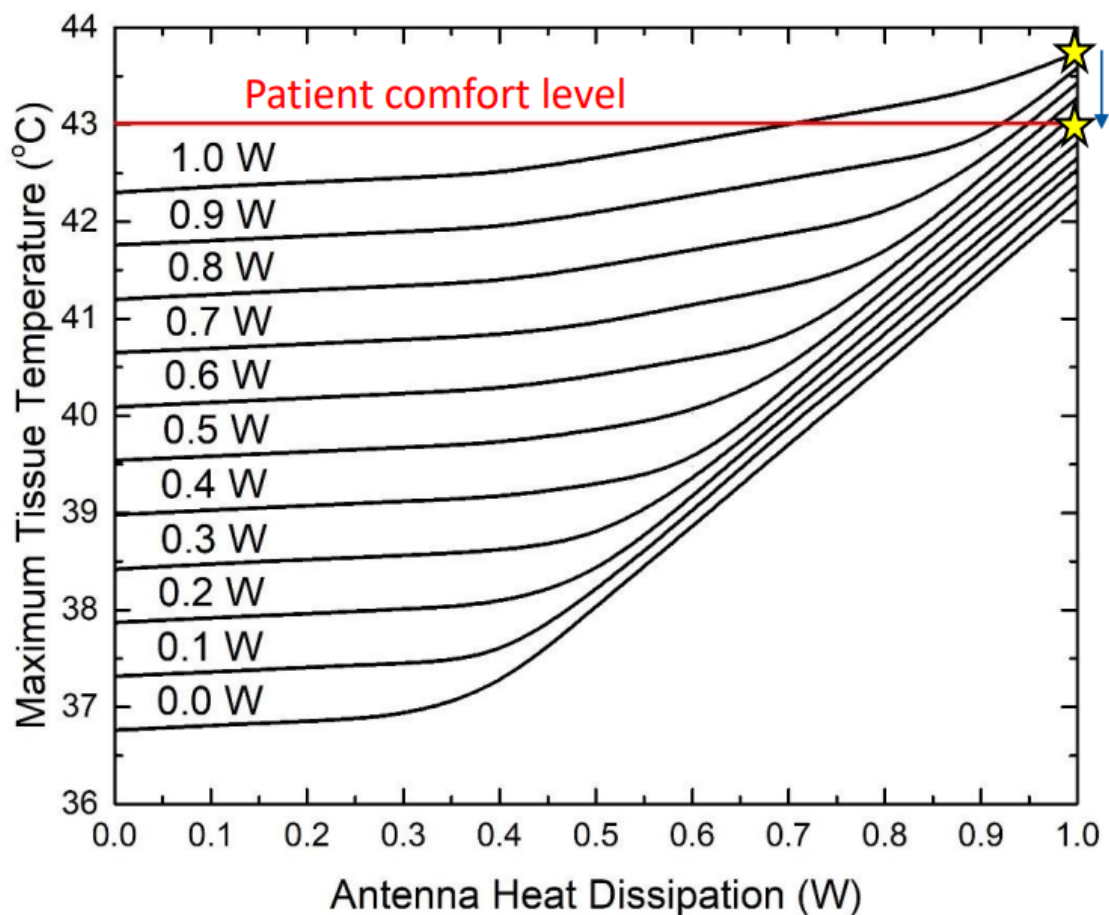


Figure 3-5: Modified version of **Figure 3-3** showing reduction in maximum tissue to below patient comfort level as denoted by red line through reduction in IPG eddy currents.

3.2.2 Antenna Modifications

Baseline results demonstrated that at high levels of heat dissipation, tissues near the antenna device are most susceptible to temperature rise above the patient comfort threshold. Targeting this component with some form of cooling solution would therefore be ideal to maximize thermal benefits near heat dissipation rates of 1 W. An active cooling scheme applied at the periphery of the antenna device consisting of some form of closed-loop water cooling or thermoelectric module was investigated for its potential at lowering tissue temperatures near the skin surface. A new boundary condition applied at the outer

rim of the antenna was imposed to simulate the cooling effect of such a device as a general outward heat flux as shown in **Figure 3-6**.

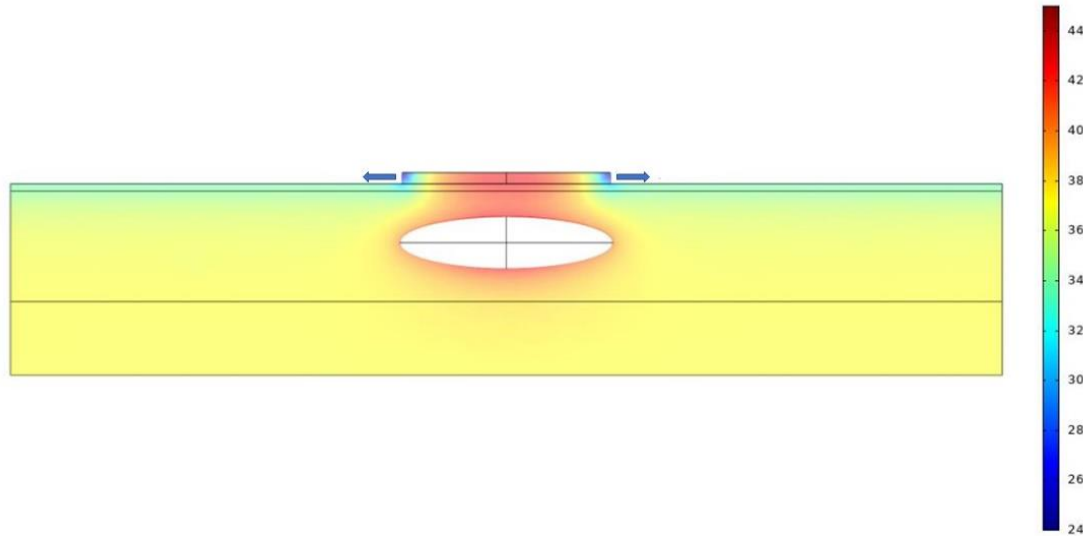


Figure 3-6: Temperature distribution with 1 W heat dissipation in the IPG and antenna and 0.8 W cooling ring represented with an imposed heat flux boundary condition directed as shown.

A cooling capacity of 0.8 W was determined as a realistic estimate for such a device that could be installed around a similarly sized antenna as the one modelled here. Baseline results without any active cooling reported a maximum temperature of 43.7 °C. The maximum tissue temperature with an 0.8 W cooling ring showed an improvement similar to that of a change of casing material for the IPG at 42.8 °C. The latter method remains the more attractive option due to the increased complexity and cost of a cooling ring as well as the additional power consumption necessary for its operation.

The final cooling solution investigated involved the use of small silicone standoffs to the underside of the antenna module to minimize thermal contact between the antenna and skin surface while not drastically increasing charging distance between the antenna and IPG as seen in **Figure 3-7**.

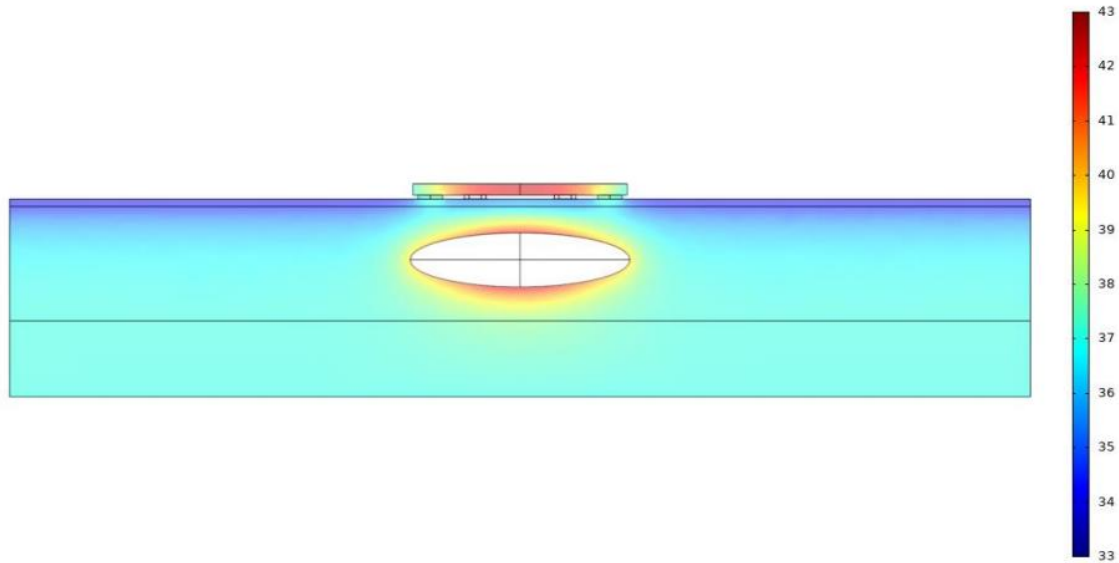


Figure 3-7: Temperature distribution with 1 W heat dissipation in the IPG and antenna with 1 mm standoffs at the base of the antenna.

To capture the thermal effects of this change in geometry in the numerical model, the same combined radiation and convective heat transfer coefficient of $10 \text{ W}/(\text{m}^2 \cdot \text{K})$ previously applied to the antenna upper surface and skin surface was applied to the additional surface area now exposed to ambient conditions. With 1 mm standoffs, maximum tissue temperature was reduced from $43.7 \text{ }^\circ\text{C}$ to $42.4 \text{ }^\circ\text{C}$ with minimal additional thermal gain past 1 mm standoff height, as seen in **Table 3-3**.

Table 3-3: Maximum Tissue Temperature at Select Surfaces with Standoff Heights Ranging from 1 mm to 5 mm

| Antenna Standoff Height (mm) | IPG Top Surface Temp (°C) | IPG Bottom Surface Temp (°C) | Skin Surface Temp (°C) | Antenna Bottom Temp (°C) |
|------------------------------|---------------------------|------------------------------|------------------------|--------------------------|
| 1 | 41.92 | 42.37 | 35.53 | 42.13 |
| 2 | 41.9 | 42.36 | 35.51 | 42.15 |
| 3 | 41.88 | 42.35 | 35.49 | 42.08 |
| 4 | 41.87 | 42.35 | 35.48 | 42.12 |
| 5 | 41.86 | 42.35 | 35.47 | 42.08 |

CHAPTER 4

CONCLUSIONS AND FUTURE WORK

4.1 Conclusion

In this work, a computational model was developed to determine the maximum temperature of tissues surrounding an inductively charged implantable neuromodulation device and skin-mounted charging antenna. A numerical model incorporating tissue layers and heat transfer due to blood perfusion according to the Pennes bioheat model was created to simulate the transient thermal response of tissues surrounding an internal pulse generator (IPG) and primary charging antenna of generic shape and size for heat dissipation rates ranging from 0.1 to 1 W within the IPG and antenna for charging times up to two hours. To gauge the validity of these results, values for maximum tissue temperature found in literature for existing devices with known heat dissipation characteristics were compared against the output of the proposed numerical model and were found to be consistent. The results of this work can therefore be leveraged by IMD researchers and designers to predict maximum tissue temperatures early in the design cycle, rather than investing valuable time and effort to a more detailed, device-specific investigation. Additionally, these results allow for IMDs with known heat dissipation profiles to be evaluated for their potential to cause patient discomfort. It was found that for tissues surrounding the IPG and charging antenna, permanent thermal damage is unlikely for the charging conditions investigated.

Thermal discomfort at high levels of device heating was found to be likely at the skin surface and was considered the upper limit of allowable heat dissipation without incorporating more advanced thermal management techniques. Several novel thermal management techniques were investigated for their potential impact in reducing maximum tissue temperature, targeting either the IPG or antenna device and incorporating both active and passive cooling schemes. Modification of the IPG geometry to increase overall surface area proved relatively ineffective in reducing overall maximum tissue temperature, showing a modest 0.1 °C reduction in maximum tissue temperature for an 11 percent increase in surface area. Change in IPG casing material was also considered for its potential in drastically reducing or eliminating eddy current generation in the outer casing, which has been shown to be a major contributor to overall heat generation during inductive charging. This proved the more promising of the two thermal management techniques considering the IPG device, reducing maximum tissue temperature to below the patient comfort threshold. Baseline results demonstrated that at high levels of heat dissipation, tissues near the antenna device are most susceptible to temperature rise above the patient comfort threshold. Targeting this component with some form of cooling solution would therefore be ideal to maximize thermal benefits near heat dissipation rates of 1 W. Two cooling schemes were considered, one consisting of a powered, closed-loop system on the periphery of the antenna, while the other focused on increasing the surface area exposed to ambient conditions through the addition of small standoffs. The latter method proved more effective, reducing maximum tissue temperatures from 43.7 °C to 42.4°C.

4.2 Future Work

The proposed thermal management techniques represent only the beginning of an effort to reduce heat dissipation in a growing array of implantable devices whose power strategies are increasingly reliant on induction technology. Current inductive charging technology for millimeter-sized implantable devices is limited by the inherent constraint of thermal losses within the system resulting in heat dissipation into surrounding tissues. In the future, a combined approach targeting both the charging antenna and implant could be studied allowing for increased power transfer rates and decreased charging time. An example of this based on results from this work could include both the addition of silicone standoffs to the antenna and a change of casing material less prone to eddy current generation. Further results might be framed in a new way, considering temperature reduction as a function of a combined thermal management strategy. Experimental studies to validate the predictions of the proposed generic model could also be undertaken to further confirm the accuracy of the proposed model in predicting *in-vivo* tissue temperature response. In terms of model improvements for future work, implanted devices in practice will have a layer of scar tissue in their vicinity after surgery. The non-isentropic nature of scar tissue compared to unscarred tissue would likely have some effect on the overall temperature distribution within the tissue but would require knowledge of its orientation and altered thermophysical properties in order to enact in a meaningful way and quantitatively determine the significance of its presence. Further, patient-specific information such as age, gender, body mass index, and tissue water content may play a role in the exact charging point in which discomfort occurs. Since this work was motivated in part to compare our results to those already in literature for detailed devices, we modeled

patient characteristics that were comparable to those studies. Thus, even if outlier patient conditions move the point of discomfort onset, it would not affect the conclusion that this modeling approach produces realistic and useful values

BIBLIOGRAPHY

- [1] C. A. Milano, A. J. Lodge, L. J. Blue, P. K. Smith, A. F. Hernandez, P. B. Rosenberg, *et al.*, "Implantable left ventricular assist devices: New hope for patients with end stage heart failure", North Carolina Med. J., vol. 67, pp. 110-115, 2006.
- [2] S. Westaby, R. Jarvik, A. Freeland, D. Pigott, D. Robson, S. Saito, P. Catarino, O.H. Frazier, "Postauricular percutaneous power delivery for permanent mechanical circulatory support," The Journal of Thoracic and Cardiovascular Surgery, Volume 123, Issue 5, pp. 977-983, 2002.
- [3] L. S. Y. Wong, S. Hossain, A. Ta, J. Edvinsson, D. H. Rivas and H. Naas, "A very low-power CMOS mixed-signal IC for implantable pacemaker applications," in IEEE Journal of Solid-State Circuits, vol. 39, no. 12, pp. 2446-2456, 2004.
- [4] G. C. Larsen, A. S. Manolis, F. A. Sonnenberg, J. R. Beshansky, N.A.Mark Estes, and S. G. Pauker, "Cost-effectiveness of the implantable cardioverter-defibrillator: Effect of improved battery life and comparison with amiodarone therapy," The Journal of the American College of Cardiology, Volume 19, No. 6, pp. 1323-1334, 1992.
- [5] U. Jow and M. Ghovanloo, "Design and Optimization of Printed Spiral Coils for Efficient Transcutaneous Inductive Power Transmission," in IEEE Transactions on Biomedical Circuits and Systems, vol. 1, no. 3, pp. 193-202, 2007.
- [6] P. Si, A. P. Hu, S. Malpas and D. Budgett, "A Frequency Control Method for Regulating Wireless Power to Implantable Devices," in IEEE Transactions on Biomedical Circuits and Systems, vol. 2, no. 1, pp. 22-29, 2008.
- [7] A. Amar, A. B. Kouki, H. Cao, "Power Approaches for Implantable Medical Devices," Sensors, vol. 15, pp. 28889-28914, 2015.
- [8] U. Jow and M. Ghovanloo, "Modeling and Optimization of Printed Spiral Coils in Air, Saline, and Muscle Tissue Environments," in IEEE Transactions on Biomedical Circuits and Systems, vol. 3, no. 5, pp. 339-347, 2009.
- [9] G. Lazzi, "Thermal effects of bioimplants," in IEEE Engineering in Medicine and Biology Magazine, vol. 24, no. 5, pp. 75-81, 2005.

- [10] J.P. Abraham, B.D Plourde, "Temperatures During Neurostimulation Recharge," *Neuromodulation: Technology at the Neural Interface*, 19: pp. 161-170, 2016.
- [11] B. Plourde, L. Vallez, B. Nelson-Cheeseman, J. Abraham, "Transcutaneous Recharge: A Comparison of Numerical Simulation to *In Vivo* Experiments," *Neuromodulation*, pp. 613-621, 2017.
- [12] Z. Wang, I. Aarya, M. Gueorguieva. *et al*, "Image-based 3D modeling and validation of radiofrequency interstitial tumor ablation using a tissue-mimicking breast phantom," *Int J CARS* 7, pp. 941–948, 2012.
- [13] M. Pavel, G. Gradinariu and A. Stancu, "Study of the Optimum Dose of Ferromagnetic Nanoparticles Suitable for Cancer Therapy Using MFH," in *IEEE Transactions on Magnetics*, vol. 44, no. 11, pp. 3205-3208, 2008.
- [14] A. Lakhssassi, & E. Kengne, & H. Semmaoui, "Modified Pennes' Equation Modelling Bio-heat Transfer in Living Tissues: Analytical and Numerical Analysis," *Natural Science*, 2010.
- [15] J. Hristov, "Bio-Heat Models Revisited: Concepts, Derivations, Nondimensionalization and Fractionalization Approaches," in *Journal of Frontiers in Physics*, Vol. 7, pp. 189, 2019.
- [16] H.H. Pennes, "Analysis of tissue and arterial blood temperatures in resting human forearm", *J. Appl. Physiol.* 1, pp. 93-122, 1948.
- [17] E. H. Wissler, "Pennes 1948 Paper Revisited," in *Journal of Applied Physiology*, Vol. 85, no. 1, pp. 35-41, 1998.
- [18] T. Campi, S. Cruciani, F. Palandrani, V. De Santis, A. Hirata and M. Feliziani, "Wireless Power Transfer Charging System for AIMDs and Pacemakers," in *IEEE Transactions on Microwave Theory and Techniques*, vol. 64, no. 2, pp. 633-642, 2016.
- [19] R. D. Lovik, J. P. Abraham, E. M. Sparrow, "Potential tissue damage from transcutaneous recharge of neuromodulation implants." *International Journal of Heat and Mass Transfer*, Vol. 52, no. 15-16, pp. 3518-3524, 2009.
- [20] J. Abraham, E. Sparrow and R. Lovik, "An investigation of tissue-temperature elevation caused by recharging of transcutaneous neuromodulation devices," 2009 Annual International Conference of the IEEE Engineering in Medicine and Biology Society, Minneapolis, MN, USA, pp. 7216-7219, 2009.
- [21] J. Stark, S. Romero, J. Gorman, J. Abraham, E. Sparrow, "Modulated-Power Implantable Neuromodulation Devices and Their Impact on Surrounding Tissue

- Temperatures,” *Journal of Biomedical Science and Engineering*, 9, pp. 545-562, 2016.
- [22] Boston Scientific. *Precision Spinal Cord Stimulator System Clinical Manual*. United States Food and Drug Administration. https://www.bostonscientific.com/content/dam/Manuals/us/current-rev-en/91083273-02_Precision_Clinician_Manual_Entrada_2_DFU_en-US_S.pdf
- [23] R. Lovik, J. Abraham, E. Sparrow, “Surrogate Human Tissue Temperatures Potential From Misalignment of Antenna and Implant During Recharging of a Neuromodulation Device,” *J Neuromodulation*;14: pp. 501–511, 2011.
- [24] F.A. Duck, *Physical properties of tissue*, A Comprehensive Reference Book, Academic Press, London, 1990.
- [25] A. Griesmer, “Size Parameters for Free Tetrahedral Meshing in COMSOL Multiphysics.”, www.comsol.com/blogs/size-parameters-free-tetrahedral-meshing-comsol-multiphysics/, 2014.
- [26] K.Frayn, , F Karpe,, B Fielding,. *et al.*, “Integrative physiology of human adipose tissue,” *International Journal of Obesity* 27, pp. 875–888, 2003.
- [27] J.P. Abraham, E.M. Sparrow, S. Ramadhyani, “Numerical simulation of a BPH thermal therapy – a case study involving TUMT,” *J Biomech Eng*, 129, pp. 548–557, 2007.
- [28] M. Mendlwitz, “The specific heat of human blood”, *Science*, 107, pp. 97-98, 1948.
- [29] J. Cutnell, K. Johnson, *Physics*, Fourth Edition. Wiley, pp. 308, 1998.
- [30] P. L. Ricketts, A. V. Mudaliar, B. E. Ellis, C. A. Pullins, L. A. Meyers, O. I. Lanz, E. P. Scott, T. E. Diller, “Non-invasive blood perfusion measurements using a combined temperature and heat flux surface probe,” in *International Journal of Heat and Mass Transfer*, Volume 51, Issues 23–24, pp. 5740-5748, 2008.
- [31] D. Brajkovic, M.B Ducharme., “Confounding factors in the use of the zero-heat-flow method for non-invasive muscle temperature measurement,” *Eur J Appl Physiol* 94, pp. 386–391, 2005.
- [32] J.J. Weinmann, E.M. Sparrow, “Heat Flow from Rechargeable Neuromodulation Systems into Surrounding Media,” *Neuromodulation: Technology at the Neural Interface*, 12: pp. 114-121, 2009.

- [33] A.R. Moritz, F.C. Henriques, “Studies of Thermal Injury: II. The Relative Importance of Time and Surface Temperature in the Causation of Cutaneous Burns. *Am J Pathol*; 23: pp. 695–720, 1947.
- [34] B. L. Viglianti, M. W. Dewhirst, J. P. Abraham, J. M. Gorman, E. M. Sparrow, “Rationalization of Thermal Injury Quantification Methods: Application to Skin Burns,” *Burns*, Volume 40, Issue 5, pp. 896-902, 2014.
- [35] H. Zhang, A. Hedge, “Overview of Human Thermal Responses to Warm Surfaces of Electronic Devices,” *ASME. J. Electron. Packag.*; 139, 2017.
- [36] R. Defrin, M. Shachal-Shiffer, M. Hadgadg, C. Peretz, “Quantitative Somatosensory Testing of Warm and Heat-Pain Thresholds: The Effect of Body Region and Testing Method,” *Clin. J. Pain*, 22(2), pp. 130–136, 2006.
- [37] H. Zhang, A. Hedge, B. Guo, “Surface and Indoor Temperature Effects on User Thermal Responses to Holding a Simulated Tablet Computer,” *ASME J. Electron. Packag.*, 138(3), 2006.
- [38] A.M. Stoll, L.C. Greene, “Relationship Between Pain and Tissue Damage Due to Thermal Radiation,” *J Appl Physiol*; 14, pp. 373– 82, 1959.
- [39] K. Buettner, “Effects of Extreme Heat and Cold on Human Skin. III. Numerical Analysis and Pilot Experiments on Penetrating Flash Radiation Effects,” *J Appl Physiol*; 5, pp. 207–20, 1952.
- [40] J. Hardy, “Thresholds of Pain and Reflex Contraction as Related to Noxious Stimulation,” *J Appl Physiol*; 5, pp. 725–39, 1959.